Aseismic slip transients emerge spontaneously in three-dimensional rate and state modeling of subduction earthquake sequences

Yajing Liu
Department of Earth and Planetary Sciences, Harvard University, Cambridge, Massachusetts, USA

James R. Rice
Department of Earth and Planetary Sciences and Division of Engineering and Applied Science, Harvard University, Cambridge, Massachusetts, USA

Received 7 September 2004; revised 6 April 2005; accepted 27 April 2005; published 16 August 2005.

[1] To investigate the possible physical mechanisms of recently observed aseismic slip events in the Cascadia, Japan and Mexico subduction zones, we apply a Dieterich-Ruina rate and state friction law to a three dimensional model of a shallow subduction fault. That is loaded by imposed steady plate slip rate far downdip along the thrust interface. Friction properties are temperature and hence depth-dependent, such that sliding is stable at depths below about 30 km. The system is perturbed into a significantly nonuniform slip mode along strike by introducing small along-strike variations in the constitutive parameters a and $(a - b)$. In addition to large heterogeneous earthquake slip at seismogenic depths, and associated postseismic transients, we found that slip events which have clearly aseismic slip rates emerge spontaneously around the downdip end of the seismogenic zone. Both transients which start well after a seismic event, and those which are triggered by other transients, are observed from the simulations. The slip velocity, depth range, and, sometimes, along-strike migration speed of simulated transients are similar to the observations from natural subduction zones. Unstable-stable transitional friction properties near the downdip end of the seismogenic zone are suggested to be an ingredient allowing such transients. Simulated transients can weaken the locking intensity of the updip seismogenic zone, while enhancing that of the transition zone. Spatial-temporal correlation of aseismic transients and nearby seismicity in the Guerrero, Mexico, area suggests that transients may signal a period of increased probability for nucleating their high-frequency counterparts, as damaging subduction thrust events.

Citation: Liu, Y., and J. R. Rice (2005), Aseismic slip transients emerge spontaneously in three-dimensional rate and state modeling of subduction earthquake sequences, *J. Geophys. Res.*, *110*, B08307, doi:10.1029/2004JB003424.

1. Introduction

[2] Recent high-resolution GPS studies of crustal movements have suggested that slow or silent slip events occur along the downdip end of the seismogenic zone of the Japan, Cascadia and Mexico subduction zones. In 1997, about 15 GPS stations, adjacent to the Bungo channel in the western Nankai trough, detected deformations that were interpreted to result from a slow thrust slip event on the subduction interface [*Hirose et al.*, 1999; *Ozawa et al.*, 2001]. That lasted for nearly one year and released a seismic moment comparable to a M_w = 6.7 earthquake. An aseismic deformation event was also observed in the Tokai region, central Japan, since October 2000, and was still active as of late 2004, with the cumulative moment equivalent to a M_w = 7.0 earthquake by the end of 2003 [*Kawasaki*, 2004]. *Dragert et al.* [2001] reported an aseismic transient that was inferred to result from slip at depths around 40 km on the Cascadia subduction interface. As shown in Figure 1, in the summer of 1999, seven continuous GPS stations on Vancouver Island recorded the reversed movement between the Juan de Fuca and North America plates. A southeast to northwest motion is clearly seen from the correlation between detection dates and distances along the strike for these GPS stations. Furthermore, continuous observations showed these aseismic transients, which are accompanied by episodic tremor activities of a type first reported by *Obara* [2002] for Nankai, are repeated every 14 to 15 months [*Rogers and Dragert*, 2003]. Silent earthquakes were also reported to have occurred in the Guerrero seismic gap, along the segment of Cocos-North America plate interface in 1998 [*Lowry et al.*, 2001] and 2002 [*Kostoglodov et al.*, 2003]. In particular, the 2002 transient was consistent with an average slip of $\sim$10 cm and produced measurable displacements over an area of

0148-0227/05/2004JB003424$09.00

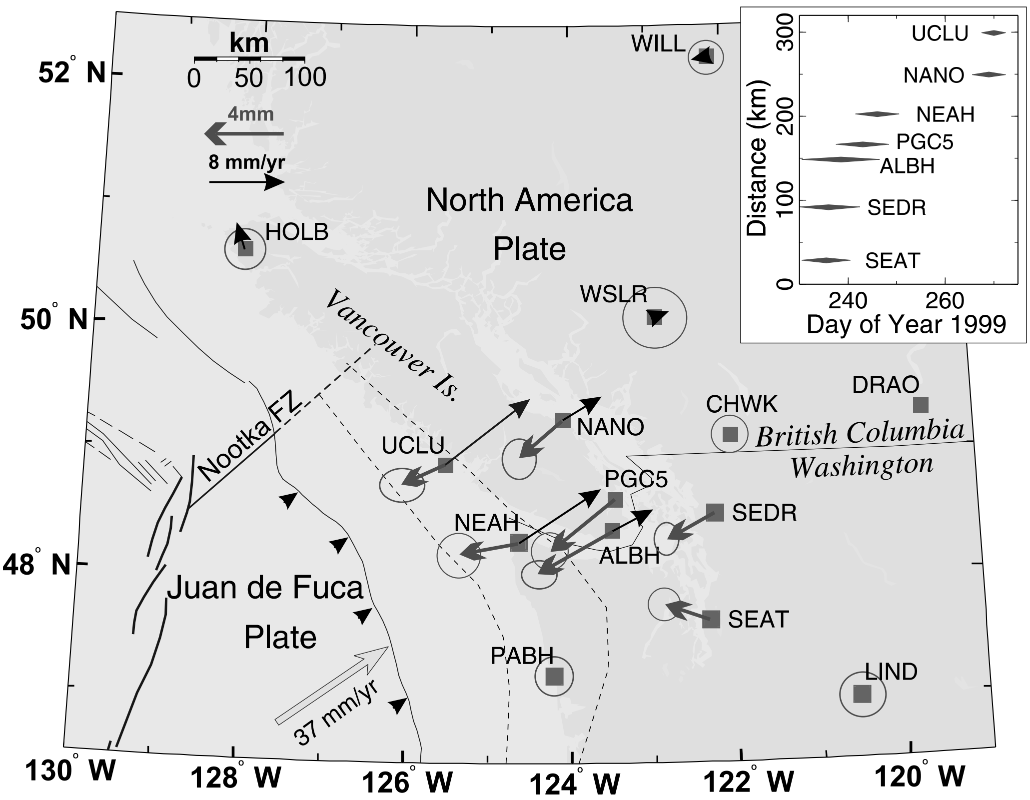

Figure 1. Locations of continuous GPS sites (from *Dragert et al.* [2001] with permission from Natural Resources Canada). Bold arrows show displacement, with respect to station DRAO, due to the aseismic slip event. Thin arrows show 3 to 6-year average GPS motions with respect to DRAO. Two dashed lines delineate the nominal downdip limits of the locked and transition zone. Inset shows the approximate time interval of the transient signal at each site along a northwest striking line.

$\sim$550 $\times$ 250 km^2, from October 2001 to May 2002. This is equivalent to a M_w = 7.5 earthquake and is considered to be the largest reliably detected silent earthquake thus far anywhere in the world [*Kostoglodov et al.*, 2003].

[3] Although such aseismic slip events were observed in different subduction zones, according to the GPS observations and inverted slip estimations from the above papers, they have some common features, which are as follows: (1) Their slip velocity, estimated from the average slips and event durations, is within the range 10^{-9} to 10^{-7} m/s [*Hirose et al.*, 1999; *Ozawa et al.*, 2001; *Dragert et al.*, 2001], which is slighter higher than the average convergence rate, typically of order 10^{-9} m/s (or, equivalently, 32 mm/yr), between the oceanic and continental plates, (2) transients migrate along the trench at speeds whose magnitude varies from kilometers per day (Cascadia and south Mexico [*Dragert et al.*, 2001; *Kostoglodov et al.*, 2003]) to kilometers per year (western Nankai, Tokai [*Ozawa et al.*, 2001, 2002]), and (3) transient slips are limited to a depth range which is near and below the downdip end of the seismogenic zone [*Dragert et al.*, 2001; *Ozawa et al.*, 2001; *Kawasaki*, 2004].

[4] Numerical simulations on the basis of rate- and state-dependent friction laws have been performed by *Tse and Rice* [1986] and *Lapusta et al.* [2000] for a vertical strike-slip fault in a two-dimensional (2-D) elastic half-space, to explain the variation of seismic slip with depth on the San Andreas Fault. Other examples, for subduction, are provided by *Stuart* [1988] for crustal deformation prior to the 1946 Nankaiko earthquake, by *Taylor* [1998, chapter VI] for dilatancy coupling to pore pressure, and by *Kato and Hirasawa* [1997] for the variation of seismic coupling along subduction zones. *Shibazaki and Iio* [2003] simulated the earthquake preparation processes using the Dieterich-Ruina friction law, to investigate the mechanism of silent slip events. They introduced a small cutoff velocity to an evolution effect in the friction law at depths below seismogenic zone, which led to their assumption of a transition from velocity weakening to velocity strengthening at low, aseismic slip rates, comparable to the plate convergence rate. However, such an assumption about the constitutive response has not yet been confirmed by laboratory studies. For example, although a transition from velocity weakening to strengthening as velocity is increased has been observed for dolomite [*Weeks and Tullis*, 1985], calcite (T. E. Tullis and J. D. Weeks, unpublished data, 1984), and, at much higher velocities, granite [*Weeks*, 1993], an opposite transition from velocity strengthening to weakening was observed in experiments on serpentinite [*Reinen et al.*, 1991, 1992] and halite [*Shimamoto*, 1986], at those low slip velocities comparable to plate velocity. In addition, all the above velocity step experiments were conducted at room temperature so that it is not clear how the cutoff velocity would vary with depth; that is an important assumption in the

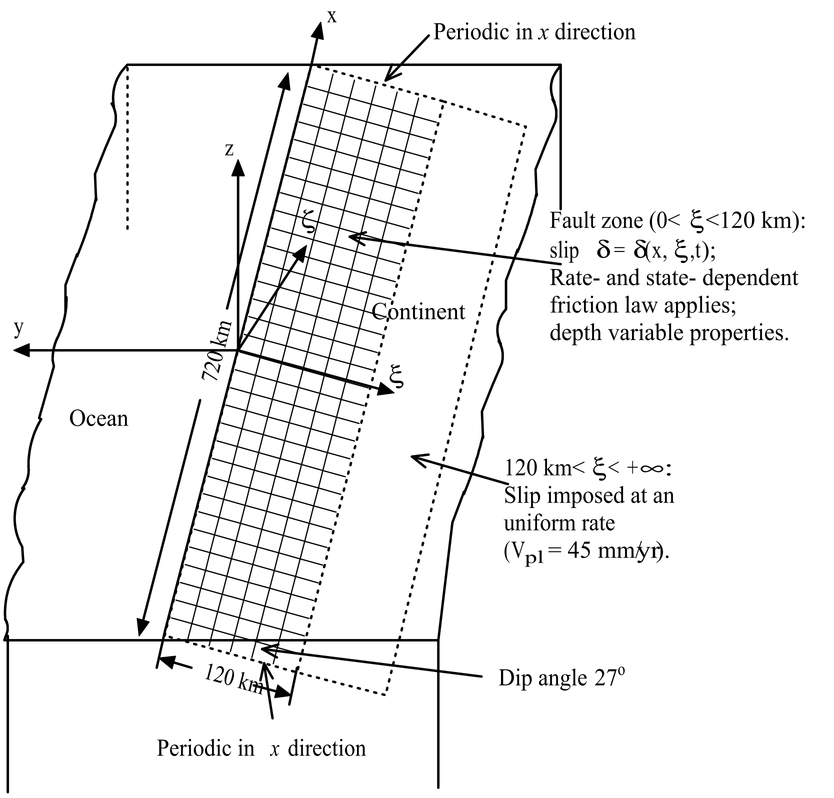

Figure 2. Geometry of the thrust fault model in an elastic half-space, driven at a uniform rate V_{pl} = 45 mm/yr below the region (0 < ξ < 120 km) in which rate- and state-dependent friction law applies. The periodic repeat distance along strike (*x* direction) is 720 km. Dip angle is chosen to be 27°.

Shibazaki and Iio [2003] modeling. For these reasons, we do not assume that feature here. Also, the fault plane used in their modeling seems, from the perspective of our present work, to be somewhat shorter than required in the along-strike direction to produce heterogeneous seismic slip histories. Simulations with along-strike length a quarter of what we used to generate results presented in this paper only result in along-strike uniformity of slip on the entire fault plane, assuming otherwise the same modeling parameters. A similar model with the cutoff velocity was presented by *Kato* [2003] for preseismic slip and slow earthquakes on the deeper extension of a subduction interface. The slow events then occurred around the downdip end of the seismogenic zone too. Because the calculation was done with a 2-D model, no along-strike variations could be examined in that study.

[5] In this paper we present a three-dimensional thrust fault model, including the Dieterich-Ruina rate- and state-dependent friction law with temperature-dependent and hence depth-dependent, properties. That applies along a thrust interface which is driven, at depths much deeper than the zone of potentially unstable friction, by imposition of a steady plate slip rate.

[6] We did not initiate the work reported here with the expectation that aseismic transients would emerge in the simulations based on such a simple model. Rather, because fluid released from metamorphic dehydration reactions has been proposed as playing an important role in causing silent slip events [*Obara*, 2002; *Rogers and Dragert*, 2003; *Kodaira et al.*, 2004], we had assumed that an extension of the modeling, which we still plan, to include transient metamorphic fluid release, and effects on pore pressure, would be needed for explanation. For example, transiently elevated pore pressure could allow episodic fault operation at low stress. Nevertheless, we find that aseismic slip events do emerge spontaneously in our simple model, with a time-independent pore pressure distribution, around the downdip end of the seismogenic zone on the subduction interface.

2. Modeling Procedures

2.1. Geometry

[7] A planar frictional interface simulates the thrust fault between a subducting oceanic plate and overlying continental plate. This is treated as a planar fault in a 3-D elastic half-space, as illustrated in Figure 2. The fault plane is defined by the *x*-ξ plane in the Cartesian coordinate system (*x*, *y*, *z*), dipping at a fixed angle θ (= 27° here) from the free horizontal surface *x*-*y*. The fault extends infinitely along strike (*x*), but the modeling is done for slip distributions which are constrained to be repeated periodically along strike with period X_l (= 720 km here; *l* denotes the along-strike direction). Slip δ(*x*, ξ, *t*) is to be calculated for a portion of the fault with $0 < \xi < W_d$ (= 120 km here; *d* denotes the downdip direction). A uniform motion at the long-term plate convergence rate V_{pl} is imposed on the depths $W_d < \xi < +\infty$, well below those of seismic activity

and postseismic transients. This $720 \times 120\ \text{km}^2$ fault plane is discretized by N_l cells along strike and by N_d cells along the downdip direction, resulting in a grid of rectangular cells with sizes $h_l = X_l/N_l$ and $h_d = W_d/N_d$. For simplicity, in the present model, we only consider slip in the downdip direction, i.e., no strike component. This extends to the subduction case the framework of 3-D strike-slip modeling with rate and state friction introduced by *Rice* [1993] and later analyzed (but with simplified mirror symmetry boundary conditions at the earth's surface) by *Rice and Ben-Zion* [1996].

2.2. Elastic Relation Between Stress and Slip

[8] Since the fault is embedded in an elastic solid, any distribution of slip motion on the fault will contribute to the shear stress distribution, and we model that according to the following "quasi-dynamic" [*Rice*, 1993] relation:

$$\tau(x,\xi,t) = -\int_0^{X_l}\int_{-W_d}^{0} k(x-x',\xi,\xi')\left[\delta(x',\xi',t) - V_{pl}t\right]dx'd\xi' - \eta\frac{\partial\delta(x,\xi,t)}{\partial t}. \tag{1}$$

The highly singular stiffness kernel $k(x - x', \xi, \xi')$ is calculated here, in discretized form, as the set of shear stresses at cell centers in Figure 2, from the quasi-static solution for a uniform slip over a rectangular dislocation on a cell centered at x', ξ' in an elastic half-space [*Okada*, 1992]. The integral in equation (1) is therefore discretized into a set of relations:

$$\tau_{ij}(t) = -\sum_{k=1}^{N_l}\sum_{l=1}^{N_d} k_{i-k,j,l}\left[\delta_{kl}(t) - V_{pl}t\right] - \eta d\delta_{ij}(t)/dt, \tag{2}$$

where subscripts i, k denote cell locations along strike, and j, l denote locations along downdip. Also, η is the radiation damping factor, following the treatment of *Rice* [1993]. It is included here to prevent the slip velocity from going unbounded during instabilities. The choice of $\eta = \mu/2c_s$, where μ is shear modulus and c_s is shear wave speed, allows equation (2) to exactly incorporate the elastodynamic result for how any instantaneous changes in $\tau_{ij}(t)$ and $d\delta_{ij}(t)/dt$ are related to each other. Equation (1) is thus dynamically correct in its instantaneous response, and in producing the long-term static response between slip and stress. It does not incorporate the wave mediated transitions between those states. Called the "quasi-dynamic" approximation, it has been shown in 2-D strike slip modeling [*Lapusta et al.*, 2000; *Lapusta and Rice*, 2003] to produce similar earthquake sequences as for fully elastodynamic modeling, but with somewhat less slip in events, and with sluggish propagation of the rupture front and slip development (e.g., minutes rather than seconds for rupture to traverse the seismogenic depth range).

2.3. Friction Law

[9] We use one of the standard laboratory-derived forms of rate- and state-dependent friction with the Dieterich-Ruina version of state variable evolution, which is thought to be in reasonable agreement with available experimental data, at least among laws including a single state variable.

Table 1. Typical Values of Parameters Chosen in Simulations

Definition	Parameter	Value
Along-strike distance	X_l	720 km
Downdip distance	W_d	120 km
Along-strike cell size	h_l	0.703 km
Downdip cell size	h_d	0.9375 km
Plate dipping angle	θ	27^o
Plate convergence rate	V_{pl}	45 mm/yr
Shear modulus	μ	30 GPa
Shear wave speed	c_s	3 km/s
Poisson's ratio	ν	0.25
Reference velocity	V_0	1 μm/s
Steady state friction coefficient at V_0	f_0	0.6
Deep effective normal stress	$\bar{\sigma}_n$	100 MPa (1000 bars)

Shear stress τ and state variable θ, which has the unit of time, evolve as in the following:

$$\tau = \bar{\sigma}_n f = \bar{\sigma}_n\left[f_0 + a\ln\left(\frac{V}{V_0}\right) + b\ln\left(\frac{V_0\theta}{L_f}\right)\right] \tag{3}$$

$$\frac{d\theta}{dt} = 1 - \frac{V\theta}{L_f}, \tag{4}$$

where f is the friction coefficient and V is the slip velocity. At steady state, when the state variable $\theta = \theta_{ss} = L_f/V$, the steady state friction coefficient is $f_{ss} = f_0 + (a - b)\ln(V/V_0)$, where f_0 is the steady state friction coefficient at rate V_0. The constitutive constants a and b are interpreted in terms of the instantaneous change in f and the steady state value of f to which it evolves (f_{ss}) in response to a step change in slip velocity: $a = V(\partial f/\partial V)_{\text{inst}}$, and $(a - b) = V(df_{ss}/dV)$. L_f (also often called d_c) is the characteristic slip distance over which the state variable evolves. $\bar{\sigma}_n = \sigma_n - p$ is the effective normal stress (the difference between normal stress and pore pressure on the fault). The assumed effective normal stress distribution is given in section 2.4. Near $V = 0$, we need to regularize the friction law to the form

$$\tau = a\bar{\sigma}_n \text{arcsinh}\left[\frac{V}{2V_0}\exp\left(\frac{f_0 + b\ln\left(V_0\theta/L_f\right)}{a}\right)\right], \tag{5}$$

as done by *Rice and Ben-Zion* [1996] [also *Lapusta et al.*, 2000; *Rice et al.*, 2001], as justified by a thermally activated description of slip at frictional contacts.

2.4. Parameter Choices

[10] A list of typical values of parameters that are chosen for the simulations shown here is included in Table 1. Where values differ from those in Table 1, their alternate values are explicitly stated in the text. Wherever possible, values of parameters are chosen to match values from appropriate laboratory experiments, or for consistency with global seismicity studies or inferences from theory, although they are constrained by considerations of computational tractability in choosing the length of L_f.

[11] The temperature dependence of the material parameter $a - b$ for granite gouge under hydrothermal conditions is shown in Figure 3a [*Blanpied et al.*, 1991, 1995]. The transition from velocity weakening ($a - b < 0$) to velocity strengthening ($a - b > 0$) around 350°C may correspond to

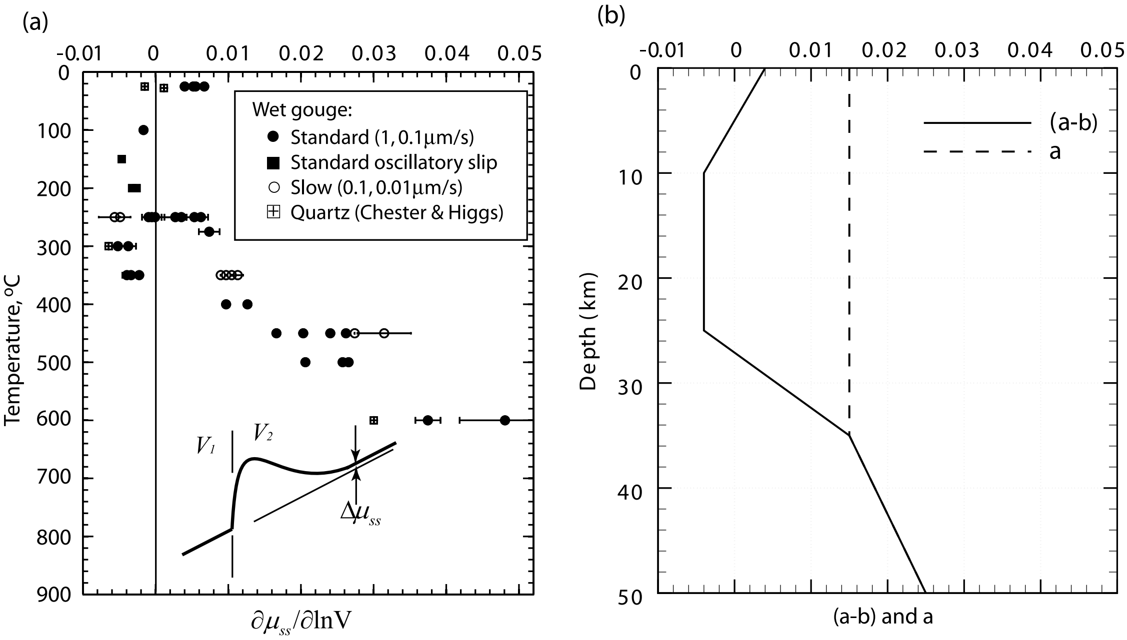

Figure 3. (a) Laboratory data, granite under hydrothermal conditions, on velocity weakening/strengthening at various temperatures (modified after *Blanpied et al.* [1995]). (b) Depth distribution of parameters a and $(a - b)$, transformed from temperature-dependent experimental data, using the thermal structure model of southwest Japan subduction zone of *Peacock and Wang* [1999].

the onset of crystal plasticity of quartz, the most ductile of the major minerals in granite [e.g., *Scholz*, 1998]. We approximate the scattered $(a - b)(T)$ data by four straight-line segments, which have ends at $(T, a - b) = (0, 0.004)$, $(100, -0.004)$, $(350, -0.004)$, $(425, 0.015)$, $(500, 0.025)$, where T is in °C. We also need to have geotherm conditions of specific subduction zones to transform the temperature-dependent a and $(a - b)$ into depth-dependent values, so that each cell on the fault can be assigned certain values of a, and $(a - b)$. *Peacock and Wang* [1999] constructed a 2-D, finite element heat transfer model for the southwest Japan subduction zone, and presented the thermal structure resulting from subduction at a rate of 45 mm/yr for 15 million years. The values of $(a - b)$ used in the modeling, Figure 3b, were determined by taking the $(a - b)$ values corresponding to those five transition temperatures at the subduction interface, and assuming temperature increases linearly with depth within each individual segment. Measurements of parameter a have been performed by *Ruina* [1980, 1983], using a servocontrol system based on a displacement measurement very near the slip surface in quartzite to simulate a highly stiff apparatus, and thus to impose abrupt slip rate changes, resulting in $a \approx 0.009$ at room temperature. A similar servocontrol system was used by *Linker and Dieterich* [1992] for granite at room temperature, and they reported $a = 0.0104 \pm 0.0007$. More recently, *Blanpied et al.* [1998] analyzed friction data from laboratory faults in granite containing gouge to explore and quantify the effects of temperature and pore water pressure on sliding behavior. They found that the direct effect a for wet granite shows a small, positive dependence on temperature, but a stronger dependence for temperatures above around 350°C. The choice of parameter a in our model (Figure 3b) reflects the mild temperature dependence noted by *Blanpied et al.* [1998] and is slightly larger (0.015 instead of 0.010) than the room temperature value.

[12] The normal stress is assumed to follow a typical overburden stress gradient, $\sigma_n = (28\ \text{MPa/km})(-z)$, and the pore pressure is given by either p = hydrostatic = $(10\ \text{MPa/km})(-z)$ or by $p = \max(\text{hydrostatic}, \sigma_n - \text{constant})$, as shown in Figure 4. The latter incorporates elevated pore pressure concepts as discussed by *Rice* [1992]. They could be appropriate for a subduction zone with fluid being released continuously by metamorphic reactions, forcing its way updip by slow permeation along the seismogenic zone and part of its downdip continuation. However, in this modeling, we regard the pore pressure as being constant with time, not transient. Typically, the constant in $p = \sigma_n$ − constant, which is the value of $\bar{\sigma}_n$ at depth, is taken in the range of 50 to 150 MPa in our simulations.

[13] A critical cell size h_d^* is defined by equating the single cell row stiffness $k_{\text{diag}}^{\text{row}} = 2\mu/\pi(1 - \nu)h_d$ for a row of cells which are not too close to the surface, to the critical spring stiffness $k_{\text{crit}} = \bar{\sigma}_n (b - a)/L_f$, in steady state slip, for a single-degree-of-freedom system following the friction law [*Ruina*, 1983; *Rice and Ruina*, 1983; *Lapusta et al.*, 2000]. That is,

$$h_d^* = \frac{2\mu L_f}{\pi(1 - \nu)(b - a)\bar{\sigma}_n}. \qquad (6)$$

To make the cells equally stiff for both along-strike and downdip rows, we require $(1 - \nu)h_d/\mu = h_l/\mu$, that is, for Poisson's ratio $\nu = 0.25$ like taken in this modeling, cells have a rectangular shape with $h_l/h_d = 1 - \nu = 3/4$ (so that $N_l = 8N_d$). To assure that the mesh is not so coarse that individual cells can act independently of one another, we require $k_{\text{diag}}^{\text{row}} \gg k_{\text{crit}}$, which in turn translates to $h_d^* \gg h_d$. For

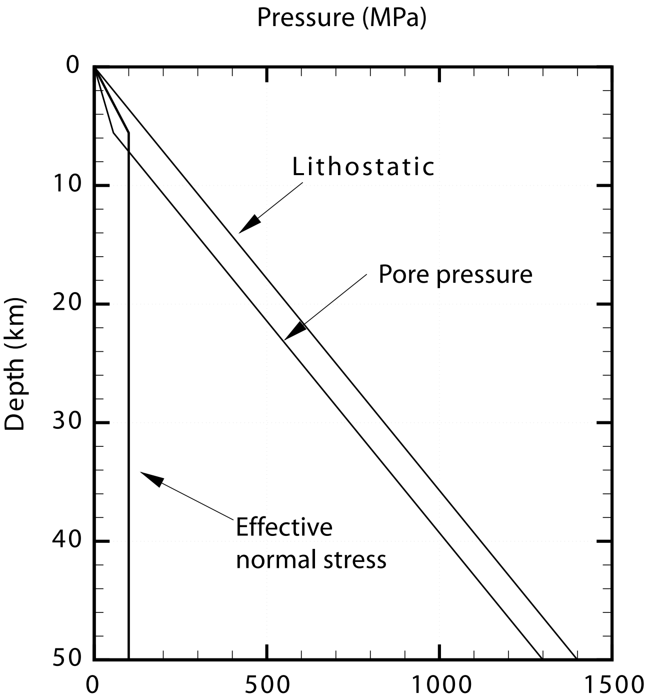

Figure 4. Depth distribution of normal stress σ_n and pore pressure p which may be hydrostatic or have a transition to increase at the same rate as for normal stress. Effective normal stress $\bar{\sigma}_n$ is the difference between normal stress and pore pressure and is typically chosen as 100 MPa in the simulation.

each simulation case shown in section 3, we give the ratio h_d^*/h_d, and the number of cells along the downdip direction N_d for the grid on which they are based, so that the value of h_d^* can be evaluated. Thus the characteristic slip distance L_f is determined by the relation

$$L_f = \frac{\pi(1-\nu)(b-a)\bar{\sigma}_n h_d^*}{2\mu}. \tag{7}$$

As in other computational simulations of this type, in order to have $h_d^* \gg h_d$ and to make simulation computationally tractable by limiting N_d and N_l, it is necessary to take h_d^* in the range of a few kilometers and then L_f in the range of cm, which is much, much larger than typical experimental values ($\sim$5 to 100 μm). The effect of such large choices have been explored [*Tse and Rice*, 1986; *Lapusta et al.*, 2000; *Lapusta and Rice*, 2003] but remain incompletely understood. Certainly, the large L_f, associated with h_d^* in the range of a few kilometers (rather than, say, 1 m), allow what seem to be unrealistically large areas of velocity weakening regions to slip stably prior to earthquake nucleation.

2.5. Computation Techniques

[14] The Runge-Kutta method with adaptive step size control is used to solve the coupled ordinary differential equations [*Press et al.*, 1992; *Stuart and Tullis*, 1995; A. Cochard, personal communication, 2002]. We can use the fast Fourier transform (FFT) to do the along-strike part of the matrix multiplications, involving stiffness matrix [k], required in each time step [*Rice*, 1993; *Stuart and Tullis*, 1995; *Rice and Ben-Zion*, 1996]. The FFT is only applied along the strike direction due to the lack of translational symmetry of the subduction geometry along the downdip direction. It reduces the computation time from scaling with $N_l^2 N_d^2$ to with $(N_l \log_2 N_l) N_d^2$. For the standard FFT implementation, the total along-strike cell number (N_l) should be chosen to be powers of 2; we use N_l = 1024 and 2048 here.

[15] The computation was done on the Harvard Division of Engineering and Applied Science computing cluster of IBM Bladecenters xSeries blades; each blade is a dual-2.4GHz Xeon processor with 2.5GB of RAM. The present algorithms are efficient between earthquakes, but require much time to integrate through earthquake instabilities. For example, with grid resolution $N_l = 2048$, $N_d = 256$, and $h_d^* = 4h_d$, $\bar{\sigma}_n$ = 100 MPa, it takes on average 2 to 3 days of full cpu time to go through one large earthquake.

3. Numerical Results and Relations to Natural Events

[16] In order to introduce arbitrary small nonuniformities along the strike direction, to perturb the system into a nonuniform slip mode, if such a nonuniform solution exists, the constitutive properties a and $a - b$ were perturbed as follows. Starting with these parameters as a function of depth as in Figure 3b, the value at each depth was reduced by 2% in the first 180 km along strike, 5% in the second 180 km, left unaltered over the next 180 km and reduced by 3% over the final 180 km of a 720-km period. Reductions in a and $a - b$ do not change the depth of velocity weakening to velocity strengthening transition over the entire fault plane. We will discuss the effect of such variations later in this section. The simulations initially start from a steady state, i.e., $V = V_{pl}$, $\theta = L_f/V$; the results shown here are parts of the simulations, taken after multiple earthquakes. To build confidence that our simulations do produce mathematically sound results rather than numerical artifacts, we conducted cases with (1) $N_l = 1024$, $N_d = 128$, $h_d^*/h_d = 4$ and (2) $N_1 = 2048$, $N_d = 256$, $h_d^*/h_d = 8$ so that both have the same h_d^* (or proportionally, the same L_f), which means we are essentially solving the same physical problem, with the same other parameters and conditions, just a fourfold greater discretization. Results from cases 1 and 2 show substantially the same slip (and slip velocity) histories over the fault plane. Therefore there are reasons for confidence that our simulations are carried out with adequate grid resolutions, at least for that h_d^*. It is difficult to be more precise on this, given that we are operating at the limits of computational tractability.

[17] Figure 5 shows the slip history of a case with N_l = 1024, $N_d = 128$, $h_d^* = 8h_d$ = 7.5 km and $\bar{\sigma}_n$ = 100 MPa, so that $L_f \approx$ 120 mm. Slip $\bar{\delta}(x, t)$ averaged over the seismogenic zone ($a - b < 0$ regime, with D_1 and D_2 as the upper and lower limits, respectively, and $D_{seismo.} = D_2 - D_1$),

$$\bar{\delta}(x,t) = \frac{1}{D_{seismo.}} \int_{D_1}^{D_2} \delta(x,\xi,t)\, d\xi, \tag{8}$$

is shown at 5-year intervals, as a function of distance x along strike from -360 km to 360 km. Results are shown

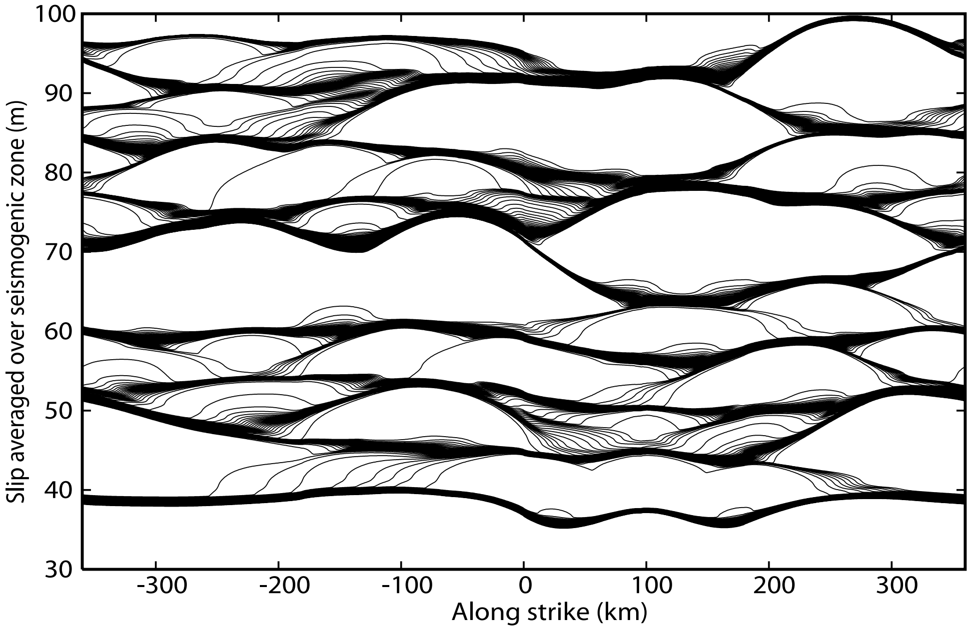

Figure 5. Slip averaged over the seismogenic zone versus distance along strike, with grid size h_l = 0.703 km, h_d = 0.9375 km, and $h_d^* = 8h_d$ = 7.5 km (so that $L_f \approx$ 120 mm). Lines are plotted for every 5 years. About 1750 years of nonuniform slip history is shown.

for a simulation of about 1750 years of calculation. We see very complex slip with strongly locked zones forming and rupturing a few times over the history. So, with small along-strike variations in frictional properties, such as a and $a-b$, the system can be perturbed into a nonuniform slip mode, generating great earthquakes, which seem to follow a broad frequency-size distribution, at different locations on the fault plane. There is no obvious correlation between the events and the sections where the small nonuniformities of parameters a and $a - b$ were introduced; significantly larger perturbations do induce such a correlation. Lateral (along-strike) variations in friction properties can produce slip heterogeneity of large earthquakes, as proposed and simulated incorporating rate and state friction by *Boatwright and Cocco* [1996]. In our 3-D simulation, however, friction parameter variation is not an essential element for along-strike heterogeneous slip. Simulations started with nonuniform initial conditions (perturbed from steady state) also generate a heterogeneous slip history.

[18] Besides great earthquakes, from this averaged slip figure we also see slowly accumulating small slips over a timescale of several tens of years, which is obviously aseismic. They are not postseismic slips because (1) postseismic slips generally occur only within a few years after the seismic event and (2) these small slips also show up at along-strike positions that are located away from the seismically ruptured areas of recent events.

[19] We examined more details of these small slip features, and observed two types of aseismic transients from our simulations.

[20] For type I, a pair of small areas with slip velocity about one order of magnitude higher than V_{pl} appears around the less well locked "gap" regions between firmly locked segments, usually tens of years after a seismic event. Snapshots in Figure 6 show the process of an aseismic transient of type I with N_l = 1024, N_d = 128, $h_d^* = 4h_d$ = 3.75 km and $\bar{\sigma}_n$ = 100 MPa ($L_f \approx$ 60 mm). Slip velocity on a log scale ($\log_{10}(V)$ with V in m/s) is plotted for the simulated fault plane. Darker contour shading represents lower slip velocity. Numbers on the top of each panel show the time (in years) after the most recent seismic event. The same plotting conventions are used in contour figures to follow.

[21] As can be seen from each snapshot in Figure 6 and later in Figures 8 and 9, near the downdip end (ξ = 120 km), the fault slips steadily at the imposed plate convergence rate V_{pl}, around 10^{-9} m/s, due to the stable velocity strengthening friction ($a - b > 0$) at the elevated temperatures of those depths. Toward the trench, the shallowest approximately 15 km of the fault undergoes slip velocity slightly lower than V_{pl}, and can accumulate small aseismic slip during the interseismic period. The regions with slip velocity of 10^{-12} or so m/s are firmly locked and considered to be healed after ruptures of previous great earthquakes.

[22] In Figure 6a, a transient starts from along-strike near positions 60 and 220 km, which are at gaps between two firmly locked regions, ~98 years after a seismic event which ruptured most of the fault (along strike 40 to −360 km and continued periodically from the top until 260 km; see the thick dark band in Figure 6). Figures 6b and 6c show the pair of slip fronts migrate toward each other along the trench. Figure 6d shows the slip fronts join at the center and reach the highest slip velocity of about 10^{-7} m/s. The transient begins to fade away in Figure 6e and completely disappears in the next couple of years. By comparing Figures 6b and 6d, an average along-strike migration speed can be estimated to be (200−140) km/(132−110) years $\approx$3 km/yr. The whole process is limited to depths below a firmly locked region (along-strike positions from 60 to 240 km). However, we notice that the locking intensity is

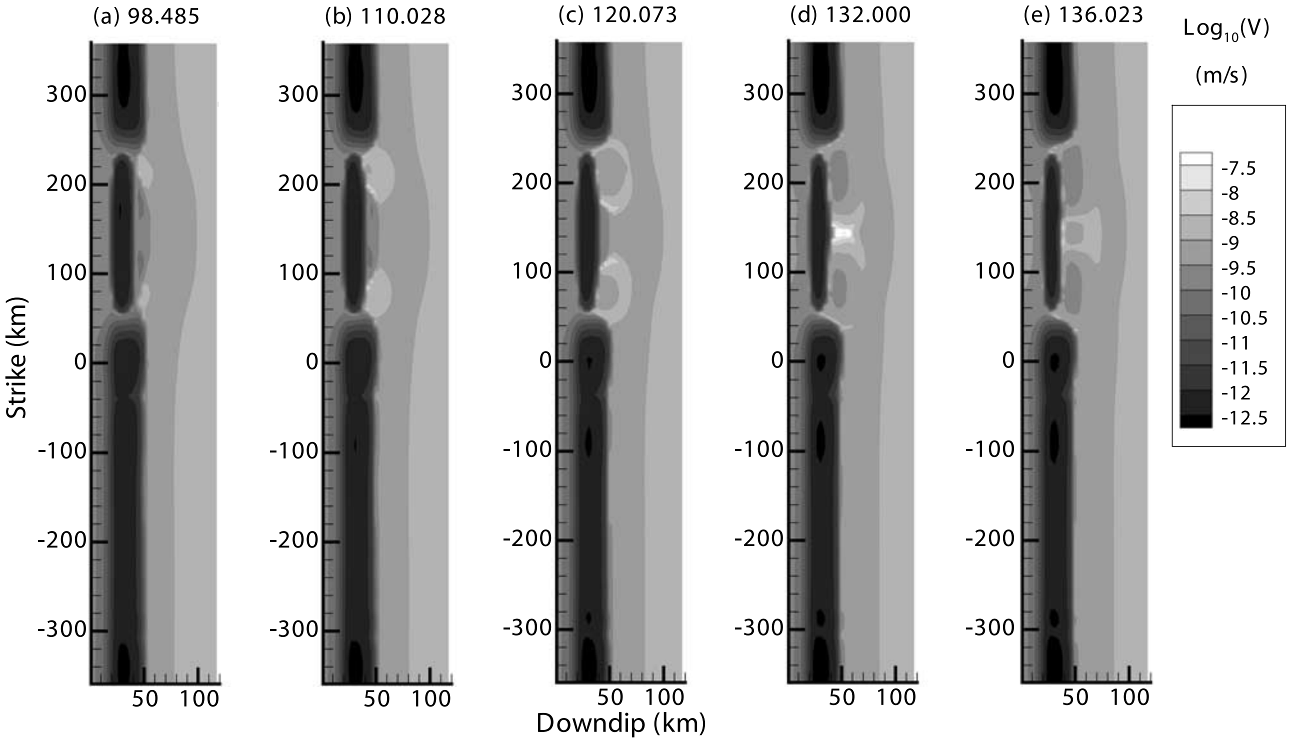

Figure 6. Snapshots of a migrating transient, simulated with grid size h_l = 0.703 km, h_d = 0.9375 km, and $h_d^* = 4h_d$ = 3.75 km (so that $L_f \approx$ 60 mm). Slip velocity (log scale in m/s) is plotted in contours on the fault plane. Numbers at top are the time in years after a most recent seismic event. Slip fronts (with velocity about 10 to 10^2 times V_{pl}) start from along-strike positions near 60 and 220 km, migrate toward each other, and join at around 140 km, where maximum slip velocity is reached.

reduced to some extent, by comparing the thickness (in the downdip direction) of that well-locked segment in Figures 6a and 6e.

[23] We may speculate that, had the great rupture zone not wrapped around from periodicity, there might have been a single rather than a pair of slip fronts which began to migrate, so that this type I process should probably not be associated uniquely with a pair of events.

[24] Figure 7 shows the slip velocity at downdip distance 50 km (near the end of seismogenic zone), represented by $\log_{10}(V/V_{pl})$, versus time right after a large seismic event, for along-strike positions 60, 220, and 140 km. They correspond approximately to the starting and joining positions of the two slip fronts, respectively. The high slip velocities at 60 and 220 km for the first $\sim$20 years are due to the postseismic effect of the prior large seismic event, while the position at 140 km was not affected because of its distance away from the seismically ruptured areas. The time window for the transient shown in Figure 6 is marked on this plot too. We can see clearly that the transient appears first at 220 km, then at 60 km a few years later, with slip velocity $\sim V_{pl}$. The maximum slip velocity ($\sim 10^3 V_{pl}$) during this transient is reached as the two fronts join at 140 km.

[25] For type II, new transients can be triggered by ongoing transients, due to stress transfer, and therefore form an almost simultaneous appearance of transients over a wide along-strike range, within a few years. Some of these newly triggered events have features, such as nucleation, propagation of the front of the faster slipping zone, and relocking, analogous to a seismic event, except that the former have much lower slip velocity (10 to 10^2 times V_{pl}) and are limited to downdip distances around 50 to 60 km in the simulations.

[26] Figure 8 shows the process of a series of triggered aseismic transients, with N_l = 2048, N_d = 256, $h_d^* = 4h_d$ = 1.875 km, and $\bar{\sigma}_n$ = 100 MPa ($L_f \approx$ 30 mm). In Figure 8a, around along-strike position 300 km and downdip 50 km, a small area with slip velocity around 10^{-8} m/s begins to develop. This area expands along strike and triggers a second transient, as can be seen in Figure 8b, around along-strike position −200 km. More transients show up in next 4 years (Figure 8c), with similar slip velocities. Aseismic "rupture" propagates along strike (Figure 8d) and the aseismically "ruptured" areas get strongly relocked after about 106 years (Figure 8e, between along-strike positions −40 km to −200 km). This is somewhat similar to the bilateral along-strike migration pattern inferred for the 2001–2002 large silent earthquake in the Guerrero seismic gap, Mexico [*Kostoglodov et al.*, 2003].

[27] Although we showed in this paper type I transients with a less refined grid N_l = 1024, N_d = 128 and type II transients with a more refined grid N_l = 2048, N_d = 256, both types can be seen in either grid resolution, and have some common characteristics which could be compared to GPS observations, as follows:

[28] 1. Transients have typical aseismic slip rates averaging around 10 to 10^2 times V_{pl}. Similar velocity magnitudes of 10^{-9} to 10^{-7} m/s have been estimated for transients in all

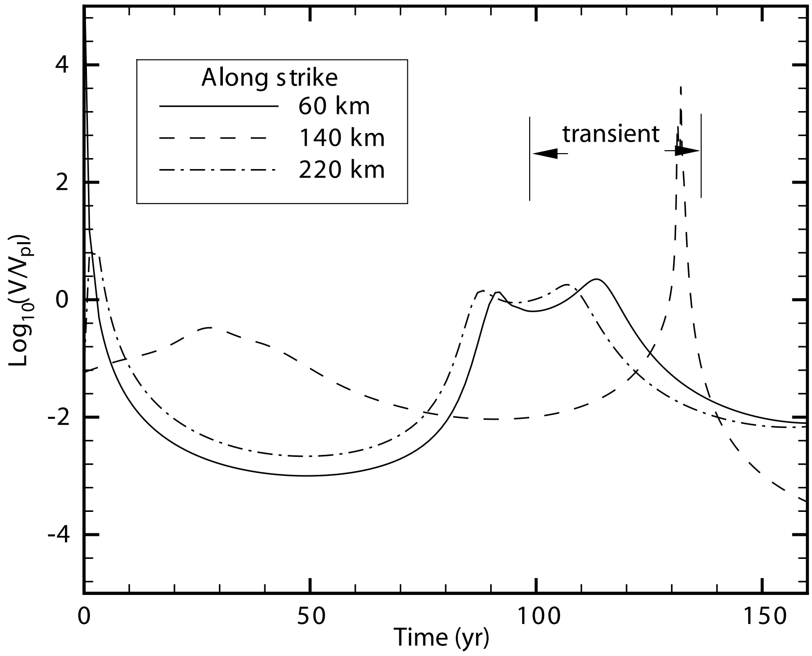

Figure 7. Slip velocity at downdip distance 50 km (near the end of seismogenic zone), at along-strike positions 60 km (solid line), 140 km (dashed line) and 220 km (dash-dotted line), with the same modeling parameters as in Figure 6. Time is after a previous seismic event. The time span for the aseismic slip event shown in Figure 6 is approximately marked by the "transient" window.

three subduction zones [*Hirose et al.*, 1999; *Ozawa et al.*, 2001; *Dragert et al.*, 2001; *Kostoglodov et al.*, 2003].

[29] 2. Transients are limited to depths around the downdip end of seismogenic zone defined in the model (Figure 3b). They generally cannot rupture into the updip portion because the fault there is very firmly locked. Nor can slip be enhanced in the velocity strengthening region that is further downdip. This depth range seems consistent

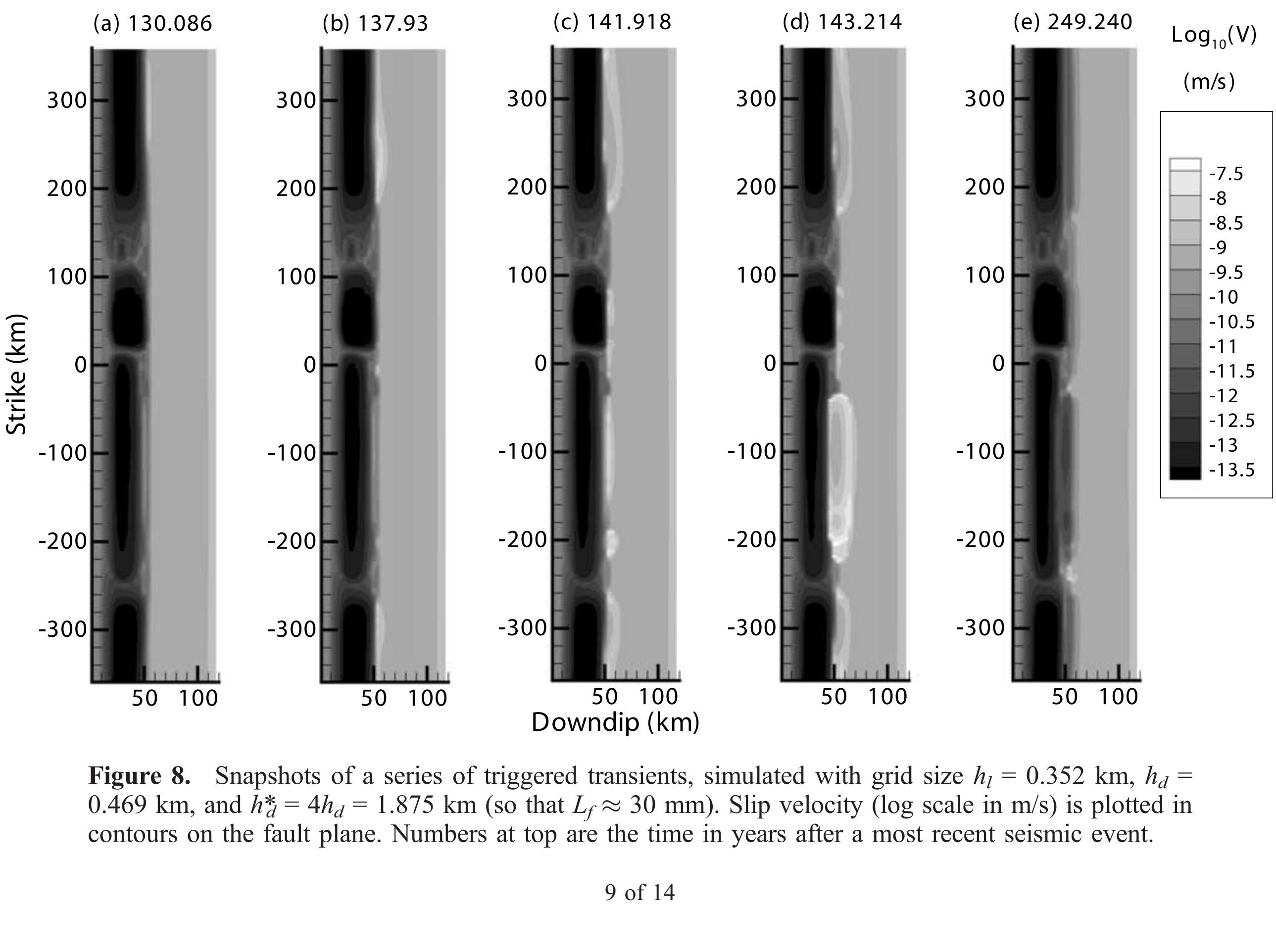

Figure 8. Snapshots of a series of triggered transients, simulated with grid size h_l = 0.352 km, h_d = 0.469 km, and $h_d^* = 4h_d$ = 1.875 km (so that $L_f \approx$ 30 mm). Slip velocity (log scale in m/s) is plotted in contours on the fault plane. Numbers at top are the time in years after a most recent seismic event.

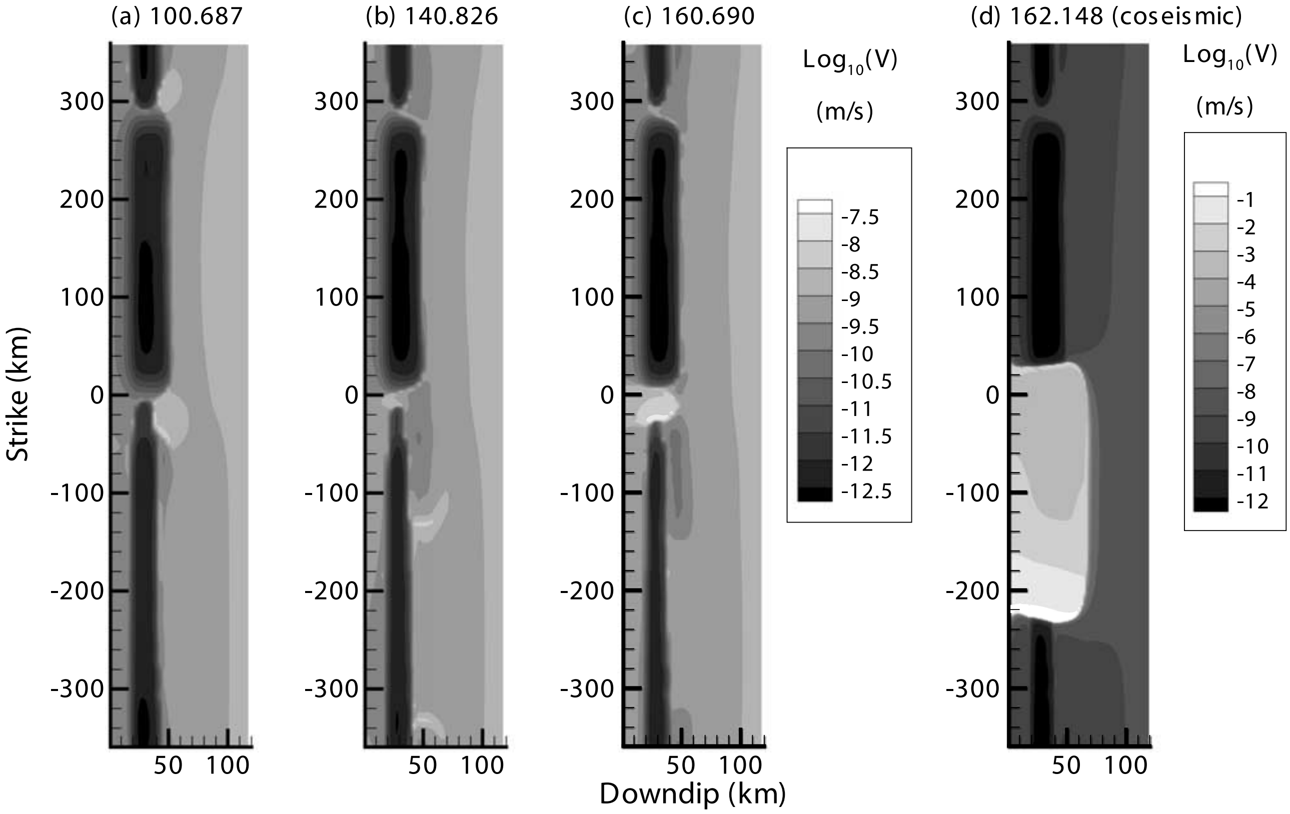

Figure 9. Snapshots of a transient which triggers a seismic event, simulated with grid size h_l = 0.703 km, h_d = 0.9375 km and h_d^* = $4h_d$ = 3.75 km (so that $L_f \approx 60$ mm), same as for the case shown in Figure 6. Different from Figure 6, the two slip fronts fade away before they meet. Instead, a large earthquake is triggered as the transient goes on. Contour legend beside Figure 9c applies only to Figures 9a, 9b, and 9c for the aseismic slip event period, and Figure 9d has a different legend (showing much higher slip rate) on the right, for the coseismic period. Numbers at the top are the time in years after a most recent seismic event.

with the observations in the Japan, Cascadia and Mexico subduction zones [*Hirose et al.*, 1999; *Ozawa et al.*, 2001; *Dragert et al.*, 2001; *Kostoglodov et al.*, 2003].

[30] 3. Transients migrate along strike at a speed of several to tens of km/yr in our simulations. As we estimated earlier, in Figure 6, the two slip fronts migrate toward each other at a speed of about 3 km/yr, before they meet and fade away. For the case in Figure 8, the migration speed is slightly faster and reaches 30 km/yr for some of the transients. The smaller characteristic slip distance L_f seems to contribute to the speed increase. This magnitude of migration speed agrees with that estimated for some transients observed in the Japan subduction zones [*Ozawa et al.*, 2001], but is much slower than the migration speeds as fast as km/day or more in the Cascadia and Mexico subduction zones [*Dragert et al.*, 2001; *Rogers and Dragert*, 2003; *Kostoglodov et al.*, 2003]. Some preliminary calculations with a higher pore pressure, thus lower effective normal stress ($\sim$ one half less), at depths seem to produce transients with modestly faster along-strike migration speeds. Possibly, modeling assumptions which allowed pore pressure to transiently approach lithostatic conditions would lead to far more rapid migration. Another possible reason is that the key modeling parameters, dip angle, plate convergence rate, geotherm, are all taken as what have been measured or computed for the southwest Japan subduction zone. Future work with parameters appropriate for the Cascadia subduction zone should be done to see if a significant increase in migration speed may occur.

4. Conclusion and Discussion

[31] We conducted three dimensional simulations of shallow subduction earthquake sequences in the framework of rate- and state-dependent friction. Aseismic slip transients, which have features such as the slip rate and depth range of occurrence in common with those observed in natural subduction zones, emerge spontaneously in the simulation results. So does along-strike heterogeneity of earthquake slip history. However, the along-strike migration speed seems compatible only with the slower events observed. Transition of frictional properties from velocity weakening to velocity strengthening, combined with great earthquake sequences that leave zones of heterogenous slip and stress alteration along strike, seem to be the cause of the aseismic slip event occurrence. They may reflect episodic relaxation, during the interseismic period, of stress concentrated around the transition zone. Our simulations suggest that hypothesis, although the detailed mechanics is far from clear to us at present. There may also be alternative, or perhaps comple-

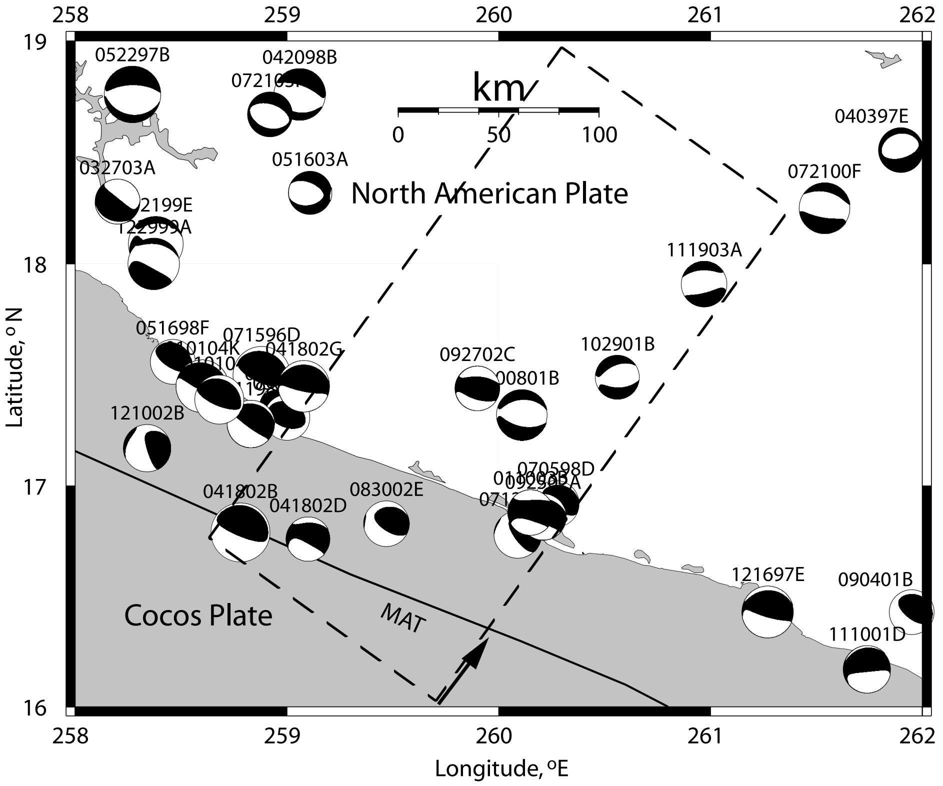

Figure 10. Seismicity from 1 May 1996 to 1 May 2004 in the Guerrero, Mexico, region from the Harvard CMT catalog; depths less than 200 km. The dashed line box aligns to the converging direction of the Cocos plate toward the North American Plate. It is drawn to approximately include the along-strike portion where large deformation due to aseismic slip events has been detected. Dates of CMT events are plotted on the top of beach balls, in the order of month, day, and year.

mentary, mechanisms for the naturally observed transients, based on episodic introduction of metamorphic fluids at high pressure along the subduction interface.

[32] For the cases shown in Figures 6 and 8, the transitional zone, where the aseismic slip is concentrated, is around 50 to 60 km along the downdip direction. In a case we tested, the distribution of friction properties with depth was altered so that the transition zone was instead set to around 60 to 70 km (10 km further downdip). As expected, occurrences of aseismic transients correspondingly shifted to the new depths of the transition zone, around 60–70 km.

[33] The occurrence of aseismic slip transients near the subduction transition zone brings up key questions for seismic hazards: How will the aseismic slip transients perturb the stress field in the seismogenic zone and will they advance or delay a future large earthquake? Our simulations suggest some complex interactions. The aseismic slip transients can release significant elastic strain energy accumulated previously around the transition zone. Their slip increases the stress on the deeper part of the locked seismogenic zone, thus possibly advancing the occurrence time of the next large earthquake. As can be seen clearly in Figure 6, the locking intensity in the seismogenic zone, where slip velocity is as low as 10^{-12} m/s, is generally weakened after the transient passes. Among the cases in our various calculations, one transient had a similar pattern to the case shown in Figure 6, with two slightly higher slip velocity fronts migrating along strike. Differently in that case, as shown in Figure 9, while the two fronts are traveling toward one another, a patch of accelerating slip appears at the along-strike position ~0 km, near one of the gaps where a transient started, and gradually become so dominant over the region that the transient fronts are suppressed before they could meet each other like in the case of Figure 6. Furthermore, that patch of accelerating slip rapidly developed into a large seismic event. A snapshot of the coseismic slip rate is shown in Figure 9d. This suggests that areas with reduced locking intensity, which naturally occur because of the along-strike heterogeneity of slip history that develops, may become potential nucleation sites for future large seismic events.

[34] A somewhat opposite effect of a transient, relative to that in Figure 6, can be seen by comparing Figures 8a and 8e. Although the locking intensity is reduced in some of the seismogenic zone, there are long regions along strike in which the transition zone becomes more firmly locked after the occurrence of a series of transients. Therefore it may become more difficult for a large seismic event to nucleate from near the downdip end of such parts of the seismogenic zone (However, in our simulations, seismic rupture seems to nucleate more frequently in downdip regions near the along-strike ends of such firmly locked sections, and they seem generally to acquire weakened locking after a transient.)

[35] A possible signature of aseismic transients in stress transfer may be noticed in the spatial-temporal seismicity variations in coupled subduction zones, such as the Middle

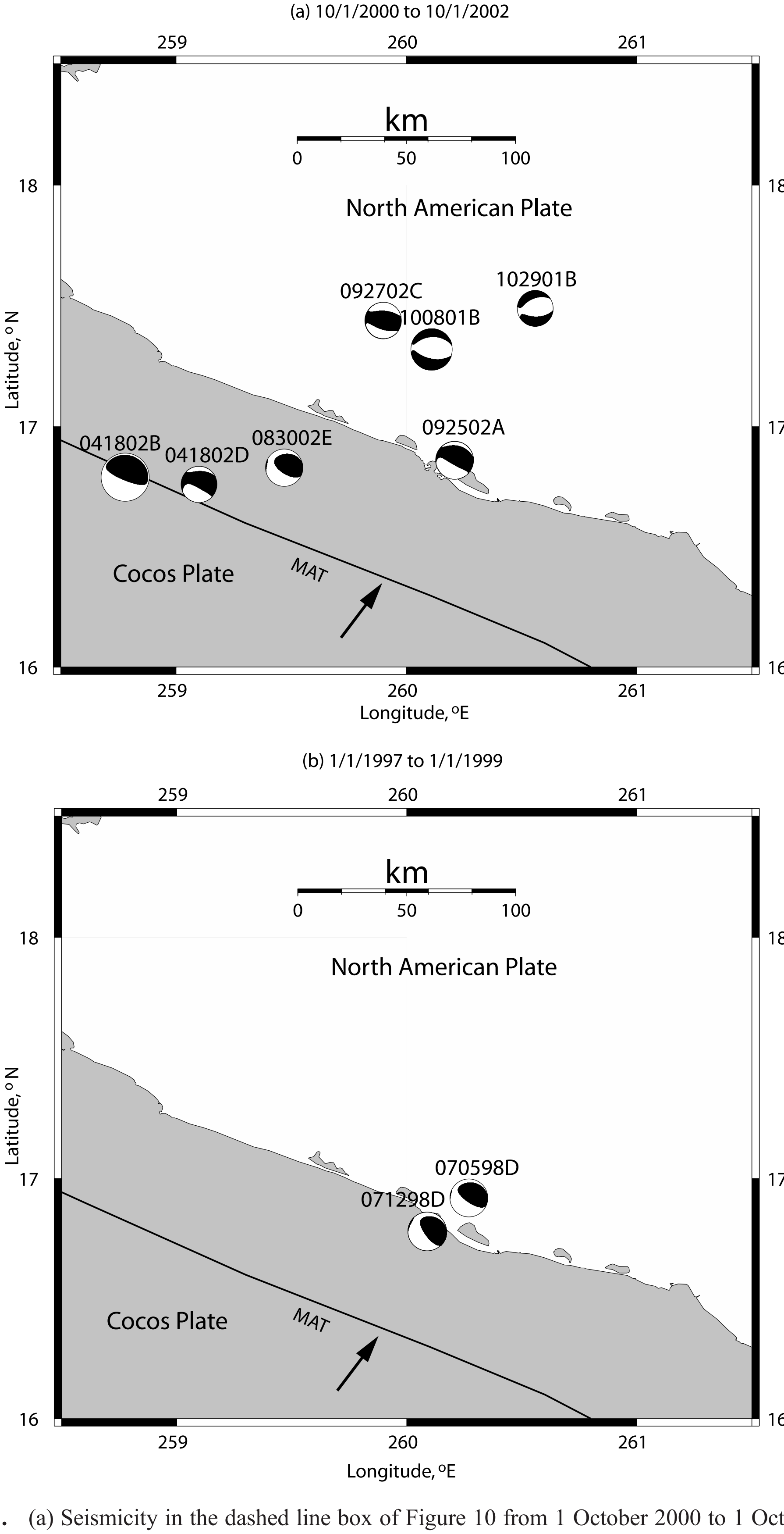

Figure 11. (a) Seismicity in the dashed line box of Figure 10 from 1 October 2000 to 1 October 2002, bracketing the transient from approximately October 2001 to April 2002. (b) Seismicity in the dashed line box of Figure 10 from 1 January 1997 to 1 January 1999, bracketing the transient from approximately January 1998 to May 1998.

American Trench (MAT) zone along Mexico. Repeated episodes of apparent switching between downdip earthquake activity in the slab and updip thrust activity have been reported by *Dmowska et al.* [1988] for regions known to have hosted large earthquakes along the MAT subduction zone. At the beginning of an episode, higher seismic activity in the downdip zone (of mainly normal faulting in the slab) coincides with relative quiescence updip in the region of the seismogenic thrust interface (where thrust events are typical). That is followed by thrust activation of the updip zone, possibly close to the area of a future main event, with relative quieting of downdip extensional activity. Then the downdip area gets activated in another episode. The direct stress influence of one seismic cluster on the other seems implausibly small, given the epicentral distance of order 100 km between them. Thus we suggest that the aseismic transients like those discussed in the paper might act as a spatial-temporal connection between the two clusters. For the 1998 and 2002 transients detected in the Guerrero, Mexico, seismic gap, there seems to be such a correlation between seismicity and transients, particularly for the larger one in 2002. Figure 10 shows the Harvard CMT events in the Guerrero area from 1 May 1996 to 1 May 2004, with depths less than 200 km. The dashed line box, aligning to the converging direction of the Cocos plate toward the North American Plate, is drawn to approximately include the along-strike portion where large deformation due to aseismic slip events has been detected. In Figure 11a, we plot the seismic events inside the dashed line box which occurred within one year before and after the start (i.e., 1 October 2000 to 1 October 2002) of the 2002 transient (approximately October 2001 to April 2002 [*Kostoglodov et al.*, 2003]). We can see that the transient was preceded, in the downdip part, by two normal events (100801B, M_w = 5.8 and 102901B, M_w = 5.0), close to the beginning of the transient, and followed in the updip part by several thrust events, including the largest one (041802B, M_w = 6.7), which coincides with the ending of the transient. This is quite similar to the pattern of *Dmowska et al.* [1988]. The evidence for such a switching pattern for the smaller 1998 transient (approximately January to May 1998 [*Lowry et al.*, 2001]) is not as prominent as for the 2002 event, considering that the only CMT normal event (040397E, M_w = 5.2) is more than 300 km away from the trench. Nevertheless, two thrust events (070598D, M_w = 5.3 and 071298D, M_w = 5.5) also occurred in the updip part several months after the transient, as shown in Figure 11b. These results suggest that transients might provide a mechanism for the otherwise enigmatic seismicity patterns of *Dmowska et al.* [1988], and also support the possibility that transients may signal a period of increased probability for nucleating their high-frequency counterparts, as damaging subduction thrust events.

[36] **Acknowledgments.** This study was supported by NSF-EAR award 0003718 on "Integrated geodetic, seismological and geodynamic studies of deformation in the Central and Southern Andes," and NSF-EAR award 0125709 on "Physically based fault zone constitutive responses and consequences for earthquake dynamics." We thank Nadia Lapusta, Alain Cochard, and Terry Tullis for their helpful suggestions and discussions on the numerical methods used in this study and Harsha Bhat and Aaron Culich for help in implementing our calculations on the parallel computing cluster, supported by the Division of Engineering and Applied Science at Harvard. We thank Renata Dmowska for advising on subduction and possible relations of transients to seismicity patterns; Herb Dragert, William Stuart, and Takane Hori for providing valuable comments at various stages of the work; and Maria E. Belardinelli, Massimo Cocco, and an anonymous reviewer for comments which helped to improve the presentation.

References

Blanpied, M. L., D. A. Lockner, and J. D. Byerlee (1991), Fault stability inferred from granite sliding experiments at hydrothermal conditions, *Geophys. Res. Lett.*, *18*(4), 609–612.

Blanpied, M. L., D. A. Lockner, and J. D. Byerlee (1995), Frictional slip of granite at hydrothermal conditions, *J. Geophys. Res.*, *100*(B7), 13,045–13,064.

Blanpied, M. L., C. J. Marone, D. A. Lockner, J. D. Byerlee, and D. P. King (1998), Quantitative measure of the variation in fault rheology due to fluid-rock interactions, *J. Geophys. Res.*, *103*(B5), 9691–9712.

Boatwright, J., and M. Cocco (1996), Frictional constraints on crustal faulting, *J. Geophys. Res.*, *101*(B6), 13,895–13,909.

Dmowska, R., J. R. Rice, L. C. Lovison, and D. Josell (1988), Stress transfer and seismic phenomena in coupled subduction zones during the earthquake cycle, *J. Geophys. Res.*, *93*(B7), 7869–7884.

Dragert, H., K. Wang, and T. S. James (2001), A silent slip event on the deeper Cascadia subduction interface, *Science*, *292*, 1525–1528.

Hirose, H., K. Hirahara, F. Kimata, N. Fujii, and S. Miyazaki (1999), A slow thrust slip event following the two 1996 Hyuganada earthquakes beneath the Bungo Channel, southwest Japan, *Geophys. Res. Lett.*, *26*, 3237–3240.

Kato, N. (2003), A possible model for large preseismic slip on a deeper extension of a seismic rupture plane, *Earth Plant. Sci. Lett.*, *216*, 17–25.

Kato, N., and T. Hirasawa (1997), A numerical study on seismic coupling along subduction zones using a laboratory-derived friction law, *Phys. Earth Planet. Inter.*, *102*, 51–68.

Kawasaki, I. (2004), Silent earthquakes occurring in a stable-unstable transition zone and impications for earthquake prediction, *Earth Planets Space*, *56*, 813–821.

Kodaira, S., T. Iidaka, A. Kato, J.-O. Park, T. Iwasaki, and Y. Kaneda (2004), High pore fluid pressure may cause silent slip in the Nankai Trough, *Science*, *304*, 1295–1298.

Kostoglodov, V., S. K. Singh, J. A. Santiago, K. M. Larson, A. R. Lowry, and R. Bilham (2003), A large silent earthquake in the Guerrero seismic gap, Mexico, *Geophys. Res. Lett.*, *30*(15), 1807, doi:10.1029/2003GL017219.

Lapusta, N., and J. R. Rice (2003), Nucleation and early seismic propagation of small and large events in a crustal earthquake model, *J. Geophys. Res.*, *108*(B4), 2205, doi:10.1029/2001JB000793.

Lapusta, N., J. R. Rice, Y. Ben-Zion, and G. Zheng (2000), Elastodynamic analysis for slow tectonic loading with spontaneous rupture episodes on faults with rate- and state-dependent friction, *J. Geophys. Res.*, *105*(B10), 23,765–23,789.

Linker, M. F., and J. H. Dieterich (1992), Effects of variable normal stress on rock friction: Observations and constitutive equations, *J. Geophys. Res.*, *97*(B4), 4923–4940.

Lowry, A. R., K. M. Larson, V. Kostoglodov, and R. Bilham (2001), Transient fault slip in Guerrero, southern Mexico, *Geophys. Res. Lett.*, *28*(19), 3753–3756.

Obara, K. (2002), Nonvolcanic deep tremor associated with subduction in southwest Japan, *Science*, *296*, 1679–1681.

Okada, Y. (1992), Internal deformation due to shear and tensile faults in a half-space, *Bull. Seismol. Soc. Am.*, *82*, 1018–1040.

Ozawa, S., M. Murakami, and T. Tada (2001), Time-dependent inversion study of the slow thrust event in the Nankai trough subduction zone, southwestern Japan, *J. Geophys. Res.*, *106*(B1), 787–802.

Ozawa, S., M. Murakami, M. Kaidzu, T. Tada, T. Sagiya, Y. Hatanaka, H. Yarai, and T. Nishimura (2002), Detection and monitoring of ongoing aseismic slip in the Tokai region, central Japan, *Science*, *298*, 1009–1012.

Peacock, S. M., and K. Wang (1999), Seismic consequences of warm versus cool subduction metamorphism: Examples from southwest and northeast Japan, *Science*, *286*, 937–939.

Press, W. H., B. P. Flannery, S. A. Teukolsky, and W. T. Vetterling (1992), *Numerical Recipes in Fortran: The Art of Scientific Computing*, 2nd ed., Cambridge Univ. Press, New York.

Reinen, L. A., J. D. Weeks, and T. E. Tullis (1991), The frictional behavior of serpentinite: Implications for aseismic creep on shallow crustal faults, *Geophys. Res. Lett.*, *18*(10), 1921–1924.

Reinen, L. A., T. E. Tullis, and J. D. Weeks (1992), Two-mechanism model for frictional sliding of serpentinite, *Geophys. Res. Lett.*, *19*(15), 1535–1538.

Rice, J. R. (1992), Fault stress states, pore pressure distributions, and the weakness of the San Andreas Fault, in *Fault Mechanics and Transport Properties in Rocks*, edited by B. Evans and T.-F. Wong, pp. 475–503, Elsevier, New York.

Rice, J. R. (1993), Spatio-temporal complexity of slip on a fault, *J. Geophys. Res.*, *98*(B6), 9885–9907.
Rice, J. R., and Y. Ben-Zion (1996), Slip complexity in earthquake fault models, *Proc. Natl. Acad. Sci. U.S.A.*, *93*, 3811–3818.
Rice, J. R., and A. L. Ruina (1983), Stability of a steady frictional slipping, *J. Appl. Mech.*, *50*, 343–349.
Rice, J. R., N. Lapusta, and K. Ranjith (2001), Rate and state dependent friction and the stability of sliding between elastically deformable solids, *J. Mech. Phys. Solids*, *49*, 1865–1898.
Rogers, G., and H. Dragert (2003), Episodic tremor and slip on the Cascadia subduction zone: The chatter of silent slip, *Science*, *300*, 1942–1943.
Ruina, A. L. (1980), Friction laws and instabilities: a quasistatic analysis of some dry frictional behavior, Ph.D. thesis, Div. of Eng., Brown Univ., Providence, R. I.
Ruina, A. L. (1983), Slip instability and state variable friction laws, *J. Geophys. Res.*, *88*, 10,359–10,370.
Scholz, C. H. (1998), Earthquakes and friction laws, *Nature*, *391*, 37–42.
Shibazaki, B., and Y. Iio (2003), On the physical mechanism of silent slip events along the deeper part of the seismogenic zone, *Geophys. Res. Lett.*, *30*(9), 1489, doi:10.1029/2003GL017047.
Shimamoto, T. (1986), Transition between frictional slip and ductile flow for halite shear zones at room temperatures, *Science*, *231*(4739), 711–714.
Stuart, W. (1988), Forecast model for great earthquakes at the Nankai Trough subduction zone, *Pure Appl. Geophys.*, *126*, 619–641.
Stuart, W., and T. E. Tullis (1995), Fault model for preseismic deformation at Parkfield, California, *J. Geophys. Res.*, *100*(B12), 24,079–24,099.
Taylor, M. A. J. (1998), Stressing, seismicity and rupture dynamics of subduction earthquakes, Ph.D. thesis, Harvard Univ., Cambridge, Mass.
Tse, S. T., and J. R. Rice (1986), Crustal earthquake instability in relation to the depth variation of frictional slip properties, *J. Geophys. Res.*, *91*(B9), 9452–9472.
Weeks, J. D. (1993), Constitutive laws for high-velocity frictional sliding and their influence on stress drop during unstable slip, *J. Geophys. Res.*, *98*(B10), 17,637–17,648.
Weeks, J. D., and T. E. Tullis (1985), Frictional sliding of dolomite: A variation in constitutive behavior, *J. Geophys. Res.*, *90*(B9), 7821–7826.

Y. Liu and J. R. Rice, Department of Earth and Planetary Sciences, Harvard University, 327 Pierce Hall, 29 Oxford Street, Cambridge, MA 02138, USA. (liu@esag.harvard.edu; rice@esag.harvard.edu)